



Review

Manufacturing and modelling of sintered micro-porous absorption material for low frequency applications

Marjaana Karhu ^{a,*}, Tomi Lindroos ^a, Seppo Uosukainen ^b^a VTT Technical Research Centre of Finland, Sinitaival 6, P.O. Box 1300, FI-33101 Tampere, Finland^b VTT Technical Research Centre of Finland, Tekniikantie 4A, P.O. Box 1000, FI-02044 VTT, Finland

ARTICLE INFO

Article history:

Received 11 December 2013

Received in revised form 13 March 2014

Accepted 10 April 2014

Available online 21 May 2014

ABSTRACT

A novel sintering based method to produce thin ultrahigh molecular weight polyethylene, UHMWPE, absorption material layer to increase absorption at low frequencies is introduced. The experimental impedance tube measurement results show that a 4 mm thick sintered sample layer increases absorption at a low frequency range below 1000 Hz compared with commercial melamine and polyester absorption foam samples. To cover a wider frequency range, multilayer structures composed of a sintered micro-porous material layer and commercial melamine and polyester foam layers are created and examined. The sintered sample layer also increases absorption in multilayer structures at low frequencies. Absorption coefficient values above 0.5 are reached starting from 200 Hz with multilayer structures. Software exploiting Biot's theory of porous materials has been adopted to fit the experimental absorption data for sintered samples, commercial foams and multilayers. Software based on Biot's theory was found to deliver quite good correlation with measured absorption coefficient values, with disagreements below 10% between the measured and estimated values.

© 2014 Elsevier Ltd. All rights reserved.

Contents

1. Introduction	151
2. Experimental procedures	151
2.1. Sample manufacturing and microstructure studies	151
2.2. Density, porosity and flow resistivity measurement	152
2.3. Sound absorption measurement	152
3. Results and discussion	153
3.1. Microstructure analysis	153
3.2. Density, porosity and flow resistivity values	154
3.3. Sound absorption	154
3.4. Sound absorption measurements of multilayers	155
3.5. Modelling prediction of sound absorption characteristics	156
3.5.1. Single layer modelling	158
3.5.2. Multilayer modelling	158
4. Conclusions	159
Acknowledgements	159
References	159

* Corresponding author. Tel.: +358 20 722 3676; fax: +358 20 7223498.

E-mail address: marjaana.karhu@vtt.fi (M. Karhu).

1. Introduction

There is strong demand for thin, lightweight and low-cost sound-absorbing materials in a wider frequency range, especially covering low frequencies. Low frequencies are problematic for traditional sound absorption materials because good absorption requires high thicknesses of the material. The research on acoustic absorption materials has mainly been on developing structures from existing materials and modelling traditional commercial absorption materials [1–4]. The sound absorption of these materials is typically high in high-frequency regions but, because of the low capacity of sound energy attenuation, the sound absorption is poor at low frequencies of several hundred Hertz. However, there have been attempts to develop completely new absorption materials. The most promising results have been achieved with micro-porous polymers, structures with dual or graded porosity [5,6]. Zhou et al. [7–10] reported that polymeric micro-spheres and micro-particles have good sound absorption capability, especially in the low frequency region. In study [8], composite material consisting of enclosed polymer micro-particles in polyurethane (PU) foam shows higher sound absorption in the low frequency region than pure PU foam with the same thickness. Study [9] looks at the properties of three polymeric micro-particle layers. Structures with a total thickness of 30 mm, consisting of a first matching layer of polystyrene particles (PS), a second matching layer of polypropylene particles (PP) and a rubber granulate layer as the sound attenuation layer, show excellent sound absorption properties for a wide frequency range. The problem is the practical use of loose particles. Swift et al. [11,12] compared loose and consolidated rubber granular mixes and pointed out that the overall absorption is reduced by the consolidation. Conducted studies indicate the possibilities of micro-particles for low frequency applications. Still there is lack of experience of consolidation techniques for producing micro-porous materials from micro-particles to be utilized in sound absorption applications.

Studies about sintering involved processing routes to produce porous polyethylene materials are presented [13,14]. Webber et al. [15] reported using the sintering and extrusion conditions

for the production of micro-porous, auxetic form UHMWPE when typically micro-porous auxetic form UHMWPE is manufactured by employing powder processing techniques including compaction, sintering and extrusion. Sintering UHMWPE particles to produce micro-porous material layer for increasing absorption at low-frequency range has not been reported previously. In this study, the novel sintering-based manufacturing route is introduced to produce thin micro-porous UHMWPE based sound absorption material layer to increase absorption in the low frequency range. To optimize the absorption characteristics in a wider frequency range, multilayer structures composed of a sintered micro-porous material layer and commercial melamine (MEL) and polyester (SD) foam layers are created and examined. Software (ESI Group NOVA) utilizing a mathematical model according to Biot's theory [16,17] for porous materials has been adopted to fit the experimental absorption data for sintered UHMWPE-based samples, commercial absorption foams and multilayers based on sintered sample layers and foam layers.

2. Experimental procedures

In this study, two types of UHMWPE powder were used to produce micro-porous sintered samples: GUR 2122-5 powder supplied by Ticona and HE 1878 powder supplied by Borealis. Microstructures of the starting powders have been examined with Scanning Electron Microscopy (SEM) and presented in Figs. 1 and 2. SEM micrographs reveal that the particle size of GUR 2122-5 powder (in Fig. 1) is much smaller than of HE 1878 (in Fig. 2) powder. Differences in powder morphologies are also detected.

2.1. Sample manufacturing and microstructure studies

A hot air sintering mould was specially designed and prepared for manufacturing sintered samples. At the first manufacturing stage, the starting UHMWPE powder was placed in the mould, which was pretreated to decrease sticking of the sample during sintering. In the second stage, the mould was placed in the oven

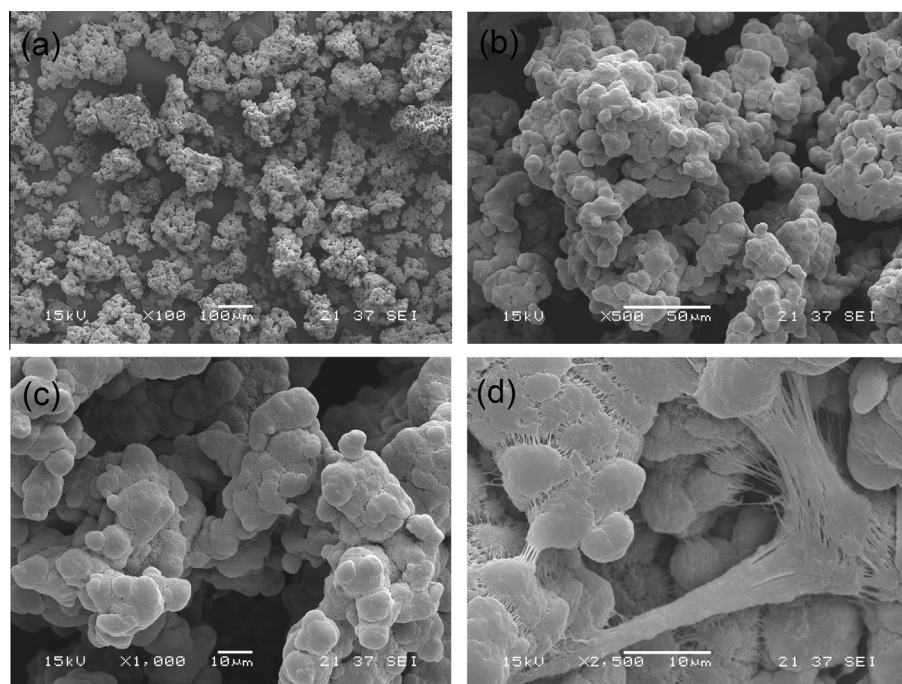


Fig. 1. SEM micrographs of Ticona GUR 2122-5 powder with magnifications: (a) 100×, (b) 500×, (c) 1000× and (d) 2500×.

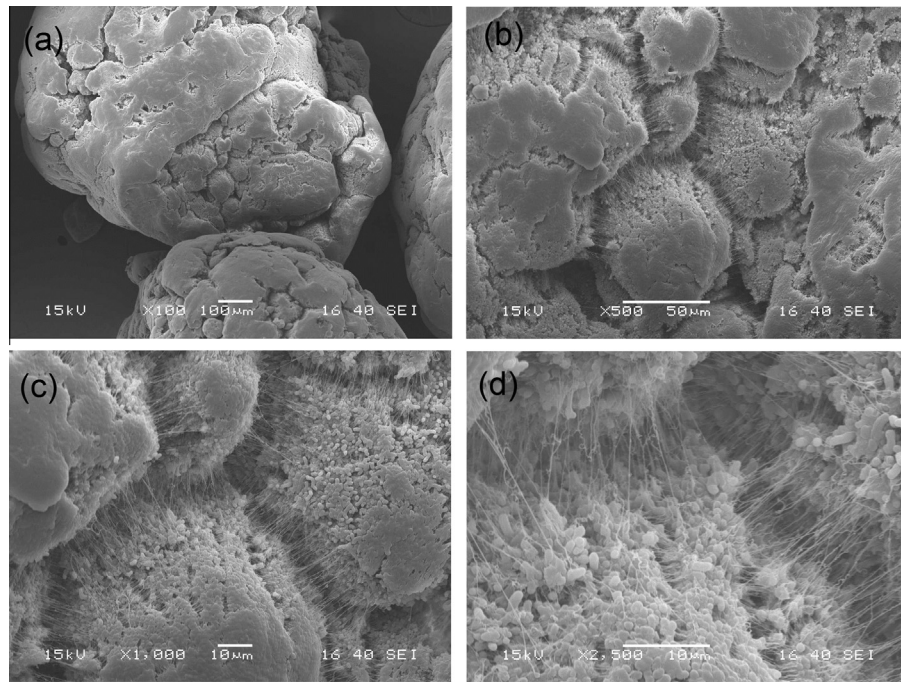


Fig. 2. SEM micrographs of Borealis HE 1878 powder with magnifications: (a) 100×, (b) 500×, (c) 1000× and (d) 2500×.

for preheating at a temperature below the sintering temperature. In the next step, to start the sintering process, hot air was blown through the mould with the selected gas flow. Finally, after sintering had taken place, the mould was immediately removed from the oven and the cooling took place at room temperature under load to minimize deformations. **Table 1** shows the detailed sintering conditions of the sintered samples: UHMWPE powder and mass, sintering temperature, time and air flow used through the sample during sintering. The fracture surfaces of the sintered samples were characterized with SEM micrographs. The samples were fractured in liquid nitrogen and coated with cold before examination in microscopy.

2.2. Density, porosity and flow resistivity measurement

Densities, ρ , of samples are defined by measuring the mass of the sample and the volume directly from the dimensions of the object. Porosity, ϕ , for absorption applications is typically defined by the ratio of the volume of the open pores to the total material volume. For the examined samples, porosity was defined by comparing the density of the object with the theoretical density of the frame material.

Table 1
Summary of the sintering conditions of the examined samples.

Sample code	Starting powder	Mass (g)	Nominal thickness (mm)	Temperature (°C)	Time (min)	Air flow (l/min)
SIN007	HE 1878	242	10	147–158	30	75
SIN017	HE 1878	112	5	145–152	40	100
SIN023	HE 1878	107	5	149–151	25	75
SIN014	GUR 2122-5	218	20	140–149	30	75
SIN010	GUR 2122-5	113	10	149–158	30	75
SIN012	GUR 2122-5	108	10	147–151	20	75
SIN013	GUR 2122-5	112	10	145–151	30	75
SIN025	GUR 2122-5	113	10	149–150	45	100
SIN018	GUR 2122-5	50	5	142–148	30	100
SIN019	GUR 2122-5	48	5	146–148	40	100
SIN024	GUR 2122-5	51	5	149–150	30	100
SIN026	GUR 2122-5	51	5	149–151	30	100

Flow resistivity, σ , is a measure of the resistance that the material offers to air flow through the material. The definition of flow resistivity, σ , is based on Darcy's law: the macroscopic velocity of the fluid in porous materials is proportional to the pressure gradient. To measure the flow resistance of the samples, a known steady airflow with velocity v was passed through the sample with a cross-section A and a thickness d while measuring the pressure difference Δp over the sample:

$$\sigma = \frac{\Delta p}{vA} \cdot \frac{A}{d} = \frac{\Delta p}{vd} \quad (1)$$

2.3. Sound absorption measurement

Sound absorption is defined as the reduction in the sound intensity through the transformation of energy to heat. The sound absorption coefficient, α , is given by the ratio of the absorbed sound intensity I_a to the incident sound intensity I_i and depends on the angle of incidence and the frequency:

$$\alpha(\theta, f) = \frac{I_a(\theta, f)}{I_i(\theta, f)} \quad (2)$$

The absorption coefficients of the examined samples have been measured according to the standard ISO 10534-2 using a Brüel & Kjaer (B&K) impedance tube. The frequency range of measures is 50–1600 Hz, but for commercial MEL and SD foams the frequency range is 50–6400 Hz. The absorption coefficient was measured under the normal incidence of the sound field and the sample was placed against a hard wall.

3. Results and discussion

3.1. Microstructure analysis

Figs. 3 and 4 show representative SEM micrographs of porous sintered samples from the UHMWPE HE 1878 powder (in Fig. 3) and UHMWPE GUR 2122-5 powder (in Fig. 4). The porous structure

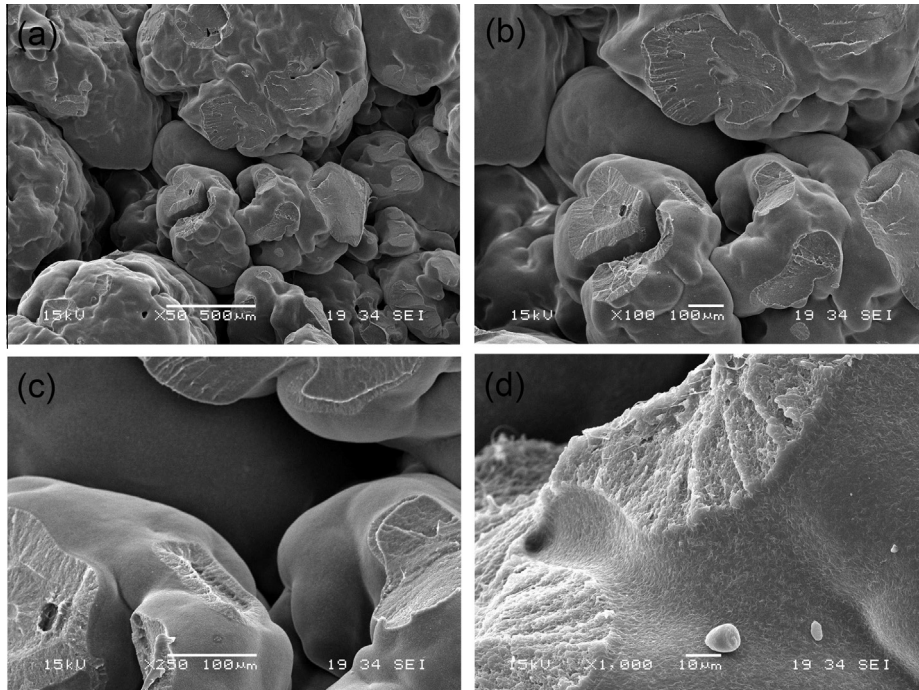


Fig. 3. Microstructure of the sintered sample from the starting powder HE 1878 with magnifications: (a) 50×, (b) 100×, (c) 250× and (d) 1000×.

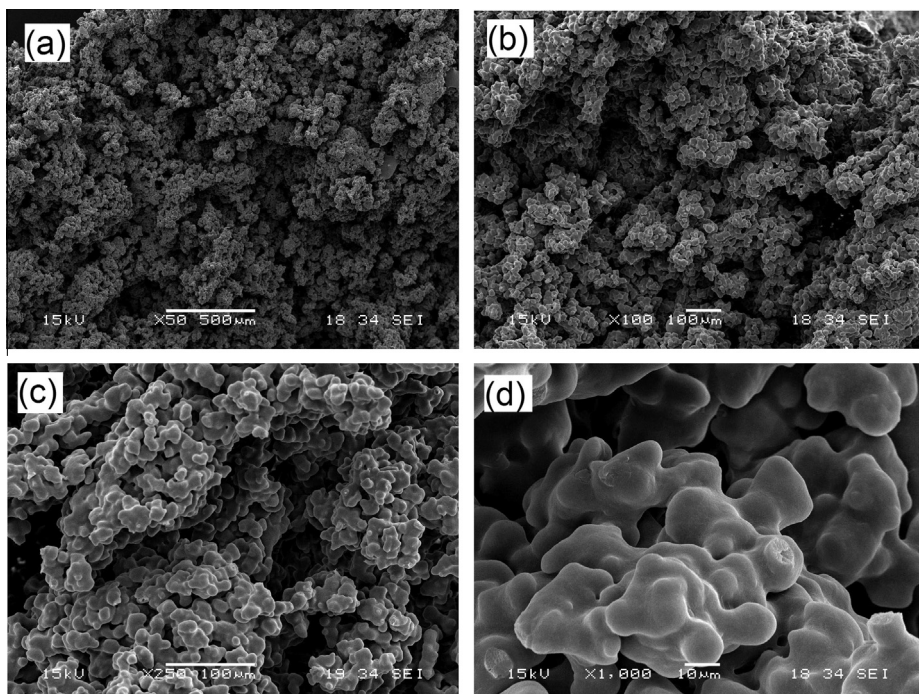


Fig. 4. Microstructure of the sintered sample from the starting powder GUR 2122-5 with magnifications: (a) 50×, (b) 100×, (c) 250× and (d) 1000×.

Table 2

Measured values for thickness, density, porosity and flow resistivity for the investigated sintered samples.

Sample code	Starting powder	Nominal thickness (mm)	Thickness (mm)	Density (kg/m ³)	Porosity	Flow resistivity (Ns/m ⁴)
SIN007	HE1878	10	9.8	578	038	88,000
SIN017	HE1878	5	5.2	500	0.46	61,000
SIN023	HE1878	5	4.5	527	0.43	90,000
SIN014	GUR 2122-5	20	20	244	0.74	320,000
SIN010	GUR 2122-5	10	8.5	293	0.69	456,471
SIN012	GUR 2122-5	10	9.3	255	0.73	408,421
SIN013	GUR 2122-5	10	9.5	264	072	400,000
SIN025	GUR2122-5	10	7.9	322	0.65	450,000
SIN018	GUR 2122-5	5	4.3	232	0.75	288,889
SIN019	GUR 2122-5	5	4.7	245	0.74	233,333
SIN024	GUR2122-5	5	4.0	242	0.74	290,000
SIN024 2x	GUR2122-5	10	8.0	242	0.74	290,000
SIN026	GUR2122-5	5	3.8	263	0.72	400,000

is seen to form between the powder agglomerations, forming irregular pores connected together and a heterogeneous distribution. HE 1878 powder with a more spherical shape results in a simpler porous structure.

3.2. Density, porosity and flow resistivity values

Table 2 shows the measured values for average thickness, density, porosity and flow resistivity for the examined sintered samples. The results show that the densities of the sintered samples from HE 1878 UHMWPE powder are higher and porosities lower than from GUR 2122-5 UHMWPE powder sintered samples. The higher densities of the HE 1878 UHMWPE powder sintered samples result from the higher bulk density of the original powder. The diversiform morphology of the original GUR 2122-5 powder compared with the more spherical morphology of the HE 1878 powder results in lower density and enables higher porosities of the GUR 2122-5-sintered samples. The flow resistivity values for the HE 1878 powder samples are almost a third of the measured values for similar thickness GUR 2122-5 samples. The lower flow resistivity values of the HE 1878 powder samples could be the result of the simpler structure of the original powder enabling easier propagation of air.

The experimental results in **Table 2** show that with nominal thicknesses of 10 mm and 20 mm, the sintered samples' density values are higher and the porosity values lower than of the 5 mm nominal thickness samples. This results from the incomplete sintering process when the thickness increases. The results exhibit difference in flow resistivity, in thickness, in density and in

porosity values for samples SIN024 and SIN026 even the samples have almost equal sintering conditions presented in **Table 1**. Besides of the particle properties the main effect of sintering process have sintering time and sintering temperature which is effecting exponentially. In addition heat conduction between particles during sintering process is complex because low thermal conductivity of polymer based particles. This effects on sintering process velocity and causes easily temperature gradients inside the sintered product. Sintering process is very sensitive mainly due to exponentially effecting sintering temperature and complexity of heat conduction between polymer based particles. Then small temperature deviations and differences in heat conduction between particles during process could effect on the final properties even if the conditions seems to be almost equal. Sample SIN026 is an example of unsuccessful sample resulting from sensitive sintering process. For that sample only small instantaneous increase of sintering temperature and deviation in heat conduction between particles resulted blocking up porous structure. This results increase in flow resistivity and density values and decrease porosity values as detected in **Table 2** for sample SIN026.

3.3. Sound absorption

Fig. 5 shows the absorption coefficients measured for HE 1878 powder sintered sample layers with nominal thicknesses of 5 mm (SIN017, SIN023) and 10 mm (SIN007) backed with an air cavity of 50 mm. High absorption with distinct peaks with an absorption coefficient value of 1 appeared around 1000 Hz for 5 mm thick sample layers. For a 10 mm thick layer, the absorption coefficient remains at a lower level, reaching a maximum of 0.85 around 600 Hz.

Figs. 6 and 7 show the absorption coefficients measured for GUR 2122-5 powder sintered sample layers with nominal thicknesses of 5 mm (SIN018, SIN019, SIN024, SIN026), 10 mm (SIN010, SIN012, SIN013, SIN025) and 20 mm (SIN014) measured with a 50 mm air gap. For thinner 5 mm nominal thickness samples (in **Fig. 6**), absorption coefficient values above 0.5 were reached starting from 250 Hz and reaching a maximum value of 0.9 around 600 Hz. For 5 mm thicker layers, absorption above 0.5 was reached after 200 Hz, reaching a distinct peak maximum of 0.8 at 300 Hz (in **Fig. 7**).

The absorption coefficient results in **Figs. 5–7** indicate that the absorption peak frequency varies with the size of UHMWPE powder used. At a low frequency range, a better absorption capability is reached with smaller size GUR 2122-5 powder.

Maa [18,19] has proposed that with micro-perforated panels, the best absorption is reached when the acoustic resistance of the micro-perforations equals the impedance of air. This behaviour results from the acoustic adjustment: if the resistance value is

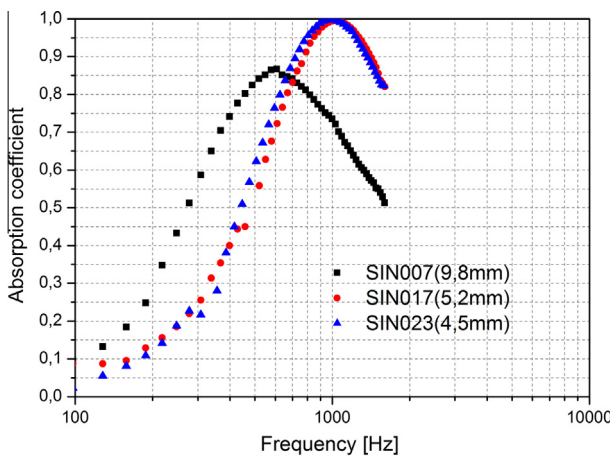


Fig. 5. Measured absorption from HE 1878 powder sintered samples with a 50 mm air gap.

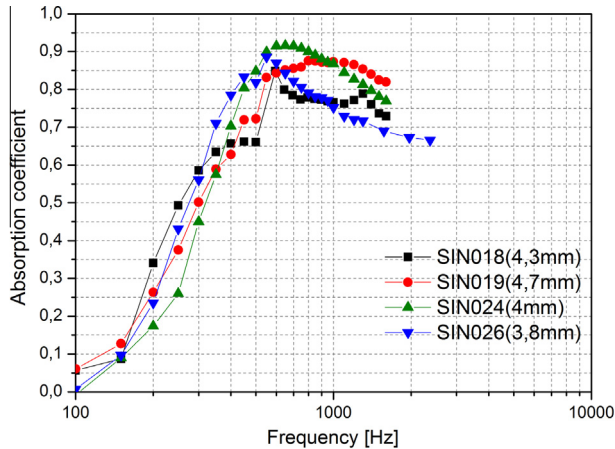


Fig. 6. Measured absorption coefficients from GUR 2122-5 powder sintered samples with a nominal thickness of 5 mm measured with a 50 mm air gap.

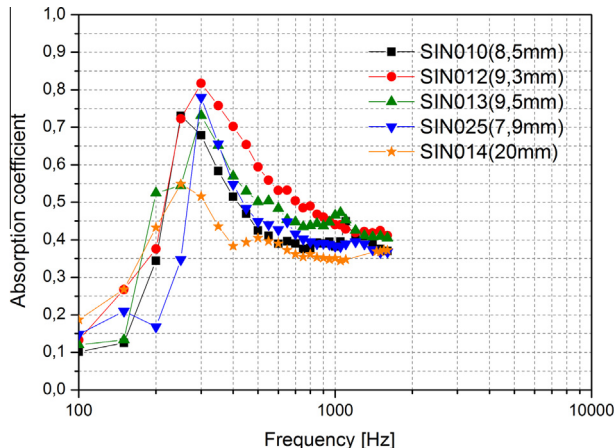


Fig. 7. Measured absorption from GUR 2122-5 powder sintered samples with nominal thicknesses of 10 mm and 20 mm measured with a 50 mm air gap.

smaller or higher than the impedance of air, the reflection increases and, at the same time, the absorption decreases. If we assume that sintered micro-porous absorption material behaves similarly to a micro-perforated panel, the acoustic resistance, z , of the material could be estimated with the equation:

$$z = \frac{\sigma * t}{Z_0} \quad (3)$$

where σ is the measured flow resistivity value, t is the thickness of the material and Z_0 is the impedance of air. In this simplified equation, it is assumed that most of the losses are generated from the flow resistance of the material. When the value of acoustic resistance, z , is equal to 1, the first absorption maximum is at the highest level. When the z value is increased, the absorption decreases but also shifts to lower frequencies, and when the z value is increased, the absorption maximum decreases and shifts to the higher frequencies. In the case of micro-porous sintered samples, the absorption maximum is reached with the SIN023 sample (in Fig. 5). The calculated z value for this SIN023 sample is close to 1 (0.98). For the sintered SIN024 sample, the calculated z value is higher (2.82), which shifts the absorption to lower frequencies (in Fig. 6).

Fig. 8 shows absorption coefficients with a 4 mm thick sintered SIN024 sample layer measured with a 50 mm air gap compared with 5 mm thick commercial MEL and SD foam measured with a 50 mm air gap. It is clearly observed that absorption by the

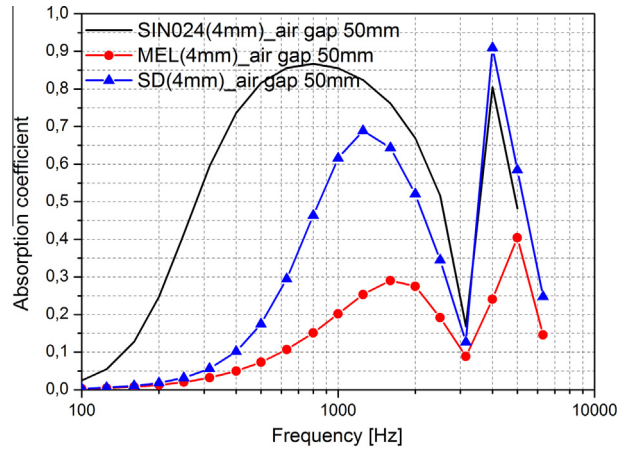


Fig. 8. Absorption coefficient reached with a 4 mm sintered sample layer compared to 4 mm MEL or SD foam layers measured with a 50 mm air gap.

sintered sample is better at a low frequency range below 1000 Hz than the absorption of the commercial foam samples.

Typically commercial absorption materials like melamine (MEL) or polyester (SD) foams are used as single layers and sound absorption is increased by increasing absorption material thickness in applications. Sintered sample layer increase absorption for low frequency range by acting as surface layer of the multi-layer structure e.g. combined to air gap or combined to other absorption material layer. To compare the actual absorbing capability in Fig. 9 comparison of a 4 mm thick sintered sample layer backed with a 50 mm air gap is made to 50 mm thick MEL and SD foam layers because the total thickness of the absorbing layers are then approximately equal. Fig. 9 result confirms that absorption of the sintered sample layer is better in low frequency range below 1000 Hz than absorption of the commercial foam samples.

3.4. Sound absorption measurements of multilayers

If only sintered sample layer absorption is exploited, an air cavity is needed behind the sintered sample layer. The production of broader and enhanced absorption region multilayer structures in which the sintered sample layer is combined with commercial MEL and SD foam layers is studied here.

Figs. 10 and 11 show impedance tube measurement results for layered structures where a 4 mm sintered SIN024 layer is backed

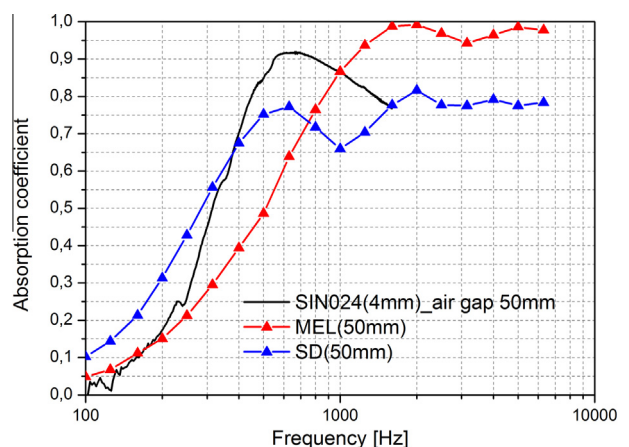


Fig. 9. Absorption coefficient reached with 4 mm sintered sample layer with 50 mm air gap compared to 50 mm MEL or SD foam layers.

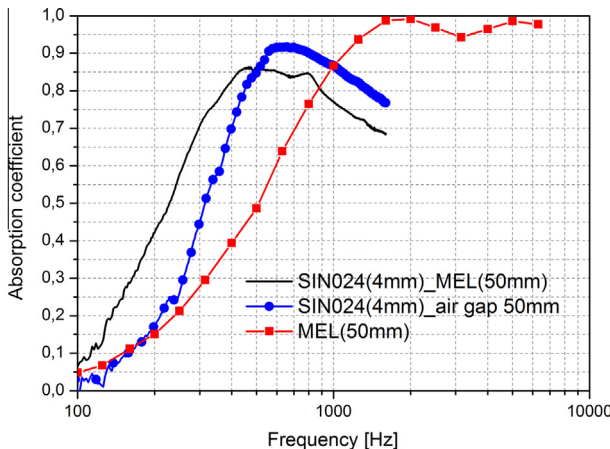


Fig. 10. Absorption of the multilayer structure SIN024(4 mm)_MEL(50 mm).

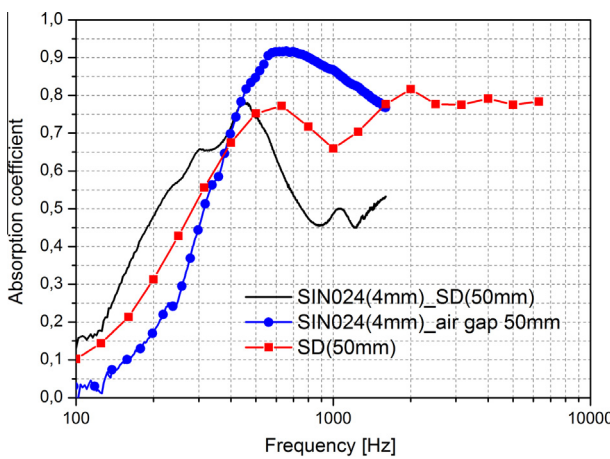


Fig. 11. Absorption of the multilayer structure SIN024(4 mm)_SD(50 mm).

with 50 mm MEL foam (in Fig. 10) and with 50 mm SD foam (in Fig. 11). For comparison, absorption coefficient measurement results for a 4 mm thick SIN024 sample backed with a 50 mm air gap and for 50 mm thick MEL and SD foam are also shown in Figs. 10 and 11. With structure SIN024(4 mm)_MEL(50 mm) (in Fig. 10), the sound absorption coefficient is enhanced in the low frequency range. An absorption coefficient above 0.5 is reached at frequencies above the 200 Hz absorption peak appearing at 500 Hz. In the case of SD foam (in Fig. 11) with a double-layer structure SIN024(4 mm)_SD(50 mm), absorption is also increased at low frequencies compared with a pure sintered SIN024 layer or SD foam layer. Absorption coefficients above 0.5 are reached at frequencies above 200 Hz. Absorption starts to decrease after a peak of 500 Hz, and a double-layer structure increases absorption only in the frequency range 200–400 Hz, but after that the absorption decreases compared with absorption with single layers. Passive sound absorption loss mechanisms affect two categories: losses in media and losses in boundaries. When they exist, losses in boundaries dominate. Losses in media include both losses in absorption

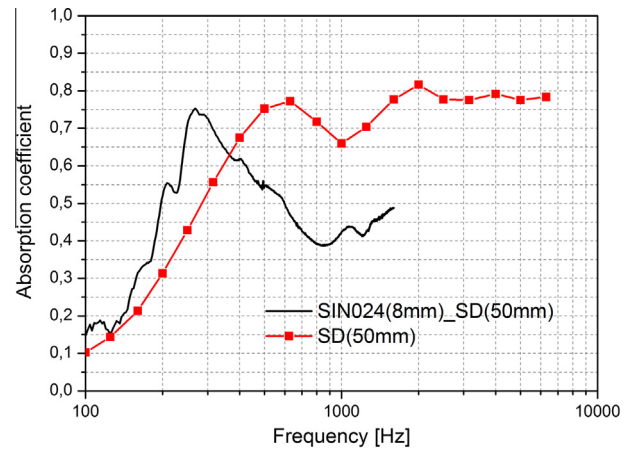


Fig. 12. Absorption of the multilayer structure SIN024(8 mm)_SD(50 mm).

material and in fluid. The loss mechanism could be divided into viscous, thermal and relaxation losses. In micro-porous materials, the effects in boundaries are enhanced because the free space between reflecting surfaces is similar in size to boundary thicknesses. In this case, the viscous and thermal losses affect all the free space between the boundaries. Viscous losses then dominate. A lower absorption coefficient and narrower absorption band with SD containing a double-layer structure compared with a MEL-containing structure could result from the effect of the higher flow resistivity value of SD foam (presented in Table 3).

Fig. 12 shows absorption coefficients measured for a multilayer structure in which two 4 mm thick sintered SIN024 sample layers are backed with 50 mm SD foam. In comparison, for absorption coefficients for a 4 mm thick sintered SIN024 layer backed with 50 mm SD foam (in Fig. 11), the absorption is increased in the frequency range 200–300 Hz but after a peak value of 0.75 at 260 Hz, the absorption decreases. If the thickness of the sintered sample SIN024 is doubled, as in the layered structure in Fig. 12, the mismatch increases, resulting in lower absorption at lower frequencies, as concluded previously based on Eq. (3). In Fig. 12 two-layer system SIN024(8 mm)_SD(50 mm) is compared with a single-layer structure SD(50 mm) to see the effect of sintered sample layer on low-frequency absorption compared to pure single layer of commercial foam.

3.5. Modelling prediction of sound absorption characteristics

Models for porous absorption materials based on different macroscopic parameters are introduced in the literature. The first models are based on empirical laws, e.g. the Delany–Bazley model [20], which is based on only one macroscopic parameter: the flow resistivity value. Porous materials consist of two phases: a solid phase ‘skeleton’ and a fluid phase that is normally air [21]. In a less complex case, the solid is motionless and only the fluid is moving. The porous material can then be modelled as a rigid porous material. In the most complex case, the solid and fluid phases are in motion simultaneously. The theoretical model that takes into consideration the movements of both phases can be found in the Biot

Table 3
Biot's parameters of examined materials used in estimations.

Porous material	Flow resistivity (Nm/s ⁴)	Density (kg/m ³)	Porosity	Tortuosity	Viscous characteristic length (m)	Thermal characteristic length (m)	Young's modulus (Pa)	Loss factor	Poisson's ratio
MEL	8000	10	0.98	1	87e-6	174e-6	200,000	0.05	0.45
SD	26,000	25	0.98	2.37	28e-6	144e-6	130,000	0.1	0.4
SIN024	290,000	242	0.74	6.9	128e-6	154e-6	9,000,000	0.05	0.3

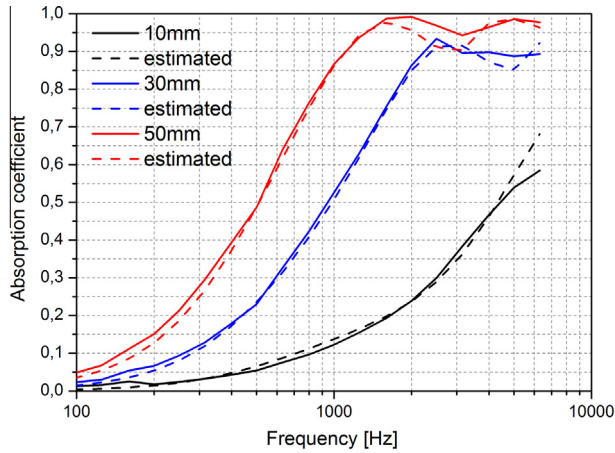


Fig. 13. Estimated and measured absorption curves for MEL.

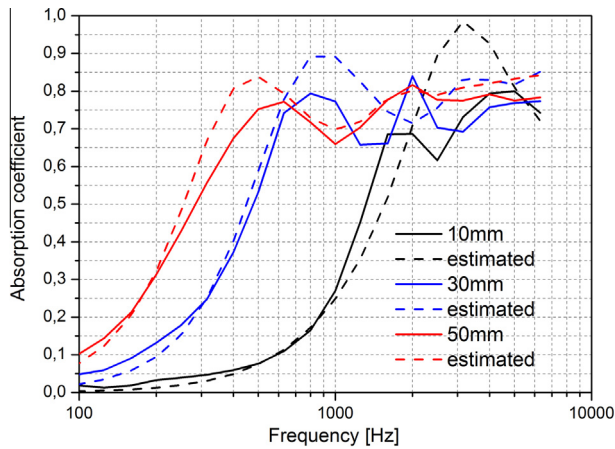


Fig. 14. Estimated and measured absorption curves for SD.

model [16,17], which is a widely accepted approach to model the performance of open-cell porous materials.

Software (ESI Group NOVA) for porous materials has been adopted to fit the experimental absorption data for the sintered material layer, commercial MEL and SD foams and multilayers presented in Section 3.4. In NOVA software, the modelling of the porous absorbents with an elastic frame is based on Biot's theory in which there is a total of nine macroscopic parameters of absorbents needed for the modelling process (flow resistivity σ , porosity Φ , tortuosity α_∞ , viscous characteristic length A , thermal characteristic length A' , density ρ , Young's modulus E , Poisson's ratio ν and loss factor η). Multilayer modelling in the software is based on using the transfer matrix method that allows modelling of multilayers containing elastic, porous elastic and fluid layers. Plane wave propagation in different media is represented with transfer matrixes. In a given layer, sound propagation is represented by a transfer matrix [T]:

$$V(M1) = [T]V(M2) \quad (4)$$

where $M1$ and $M2$ are points set close to the forward and backward face of the layer, and the components of the vector $V(M)$ are the variables that describe the acoustic field at point M of the medium. A global system of equations is formed and solved for the reflection and transmission coefficients using continuity equations at different interfaces and impedance equations in the source and receiving domains.

The density, porosity and flow resistivity of the examined porous materials are measured as described in Section 2. Young's modulus and loss factor values for the porous materials are gathered from Dynamic Mechanical Thermal Analysis (DMTA) measurements with the Mettler Toledo DMA861 device. The measurement techniques for tortuosity, viscous characteristic length and thermal characteristic length are cumbersome, and the accuracy of the results is poor. In this study, the software option (ESI Group FOAM-X) inverse characterization module is used to define the estimated values for these parameters from the impedance tube data.

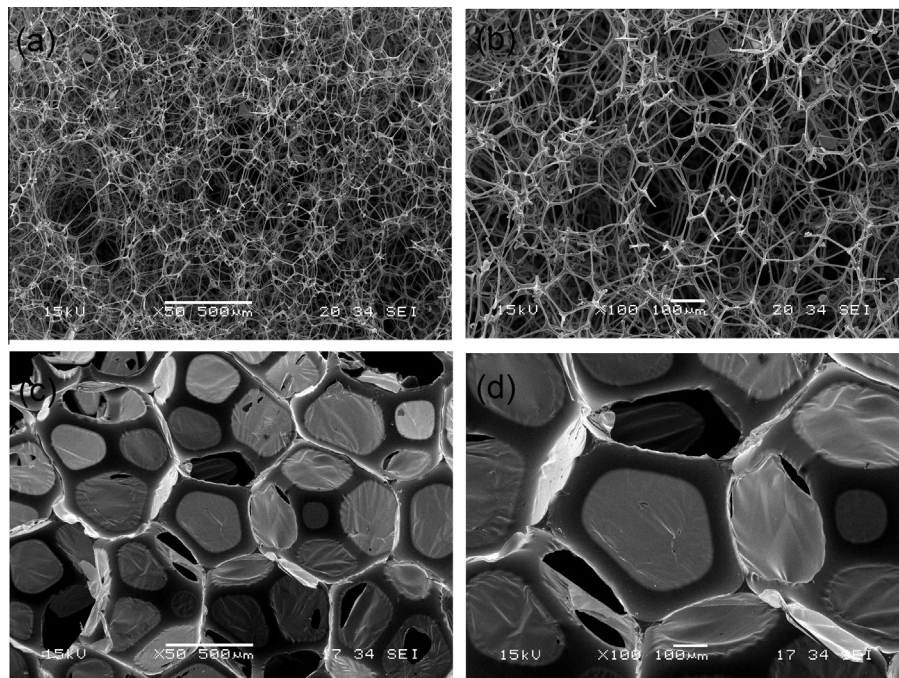


Fig. 15. Micrographs of: (a) MEL foam with 50× magnification, (b) MEL foam with 100× magnification, (c) SD foam with 50× magnification and (d) SD foam with 100× magnification.

3.5.1. Single layer modelling

Firstly, single layers of sintered sample SIN024, MEL and SD foam are estimated with the NOVA software based on nine Biot's parameters. Table 3 shows the values for these nine parameters that are needed for modelling porous materials in the NOVA software.

Figs. 13 and 14 show absorption coefficients for 10 mm, 30 mm and 50 mm thick MEL and SD samples measured in the impedance tube and estimated using rigid frame theory in the NOVA software. For the MEL foam, there is a good correlation between the measured and estimated results for the examined frequency range. For 10 mm thick SD foam, the disagreement between measured and estimated values is over 10% below 400 Hz, an average of 23% between 1250 and 1700 Hz and an average of 32% between 2500 and 4000 Hz. For 30 mm thick samples, the disagreement is over 10% below 250 Hz, an average of 14% between 800 and 2000 Hz and an average of 11% between 2500 and 3150 Hz. For 50 mm thick samples, the agreement between measured and predicted values is at the best level. The disagreement is only bigger than 10% (average 16%) between 250 and 500 Hz.

Fig. 15 shows SEM micrographs of the microstructures of MEL and SD foam. The micrographs reveal that SD foam contains foils between open pores. This could be the reason the model fitting is poorer with SD foam than with MEL foam. SD foam containing foils prevents air flow and the volume subjected to air flow is much smaller; the fitting of the model is then also poorer. With thinner samples, the accuracy of the estimation is also poorer than with thicker samples. With thinner samples, the participating volume is also smaller. The microstructure of the MEL foam, however, is homogenous, resulting in a good model fitting.

Figs. 16 and 17 show values measured with the impedance tube and estimated with the NOVA software by the Biot's theory for the sintered sample layer with different air gaps and thicknesses. Fig. 16 shows measured and estimated values for a 4 mm thick sintered sample SIN024 layer with air gaps of 50 mm, 75 mm and 100 mm. The agreement between the experimental results and estimations is satisfactory, with the disagreement being below 10% for most of the measured frequency range. The disagreement is biggest at low frequencies: with a 50 mm air gap the average disagreement is 25% for the frequency range 150–320 Hz, with a 75 mm air gap it is 26% for the frequency range 100–280 Hz, and with a 100 mm air gap it is 27% for the frequency range 100–270 Hz. Fig. 17 represents measured and estimated values for the 4 mm, 8 mm and 12 mm thick sintered sample SIN024 layers measured with a 50 mm air gap. Measurements have been made of one layer (4 mm thick), two layers (8 mm thick) and three layers

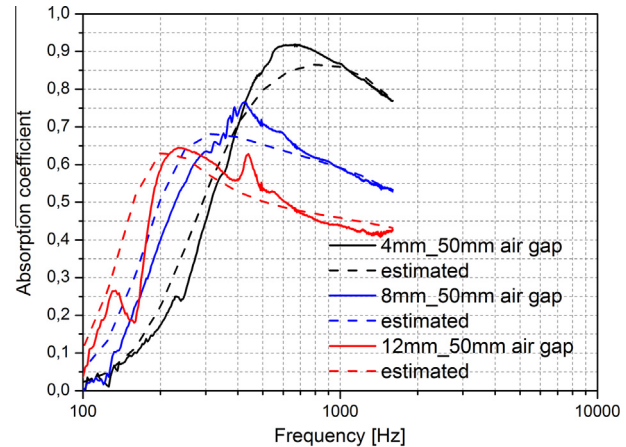


Fig. 17. Sintered SIN024 with a 4 mm sample, 8 mm sample and 12 mm sample measured and estimated absorption curves with 50 mm air gap.

(12 mm thick) of a sintered SIN024 sample. The disagreement is again biggest at low frequencies. For 8 mm layer thickness, it is on average 30% for frequencies between 100 and 274 Hz. For 12 mm layer thickness, the disagreement is biggest, on average 30%, in the frequency range 100–196 Hz and on average 15% at frequencies between 420 and 474 Hz. One explanation for the disagreement between measured and NOVA estimated values at low frequencies is inaccuracies in impedance tube measurement results at frequencies below 200 Hz, which also results in differences between measured and predicted values. In the case of the sintered sample, the NOVA software estimations are very sensitive to the measured sample thickness and measured air gap, which have been used in the calculations. To improve the agreement with experimental results, these parameters could be adjusted noting the measurement accuracy of these values. For the sintered sample, the variation in thickness is quite large (tolerance 1 mm) and the best agreement between the measured and predicted values is reached using the minimum thickness value instead of the average thickness.

3.5.2. Multilayer modelling

Figs. 18–20 show values measured with the impedance tube and estimated results with the NOVA software by the Biot's theory for the multilayer materials described in Section 3.4. Fig. 18 shows measured and estimated results for the double-layer structure with a 4 mm thick sintered SIN024 layer backed with a 50 mm

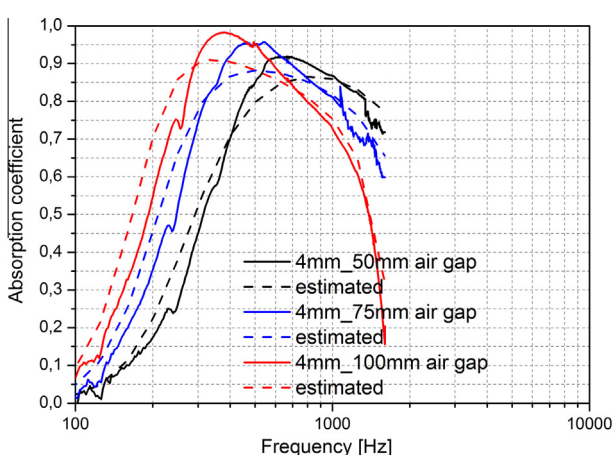


Fig. 16. Sintered SIN024 sample measured and estimated absorption curves with 50 mm, 75 mm and 100 mm air gaps.

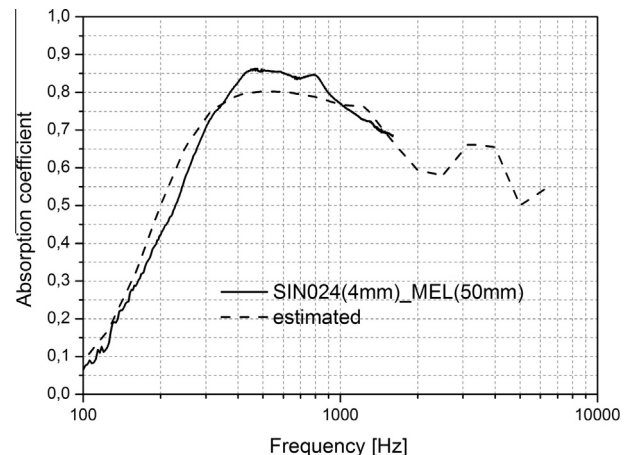


Fig. 18. Estimated and measured absorption behaviour of the layered structure SIN024(4 mm)_MEL(50 mm).

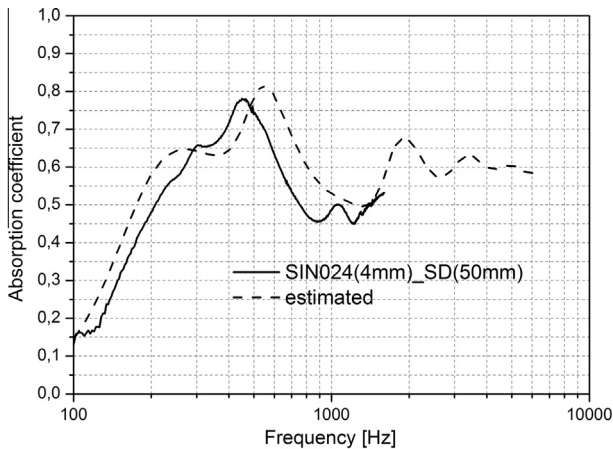


Fig. 19. Estimated and measured absorption behaviour of the layered structure SIN024(4 mm)_SD(50 mm).

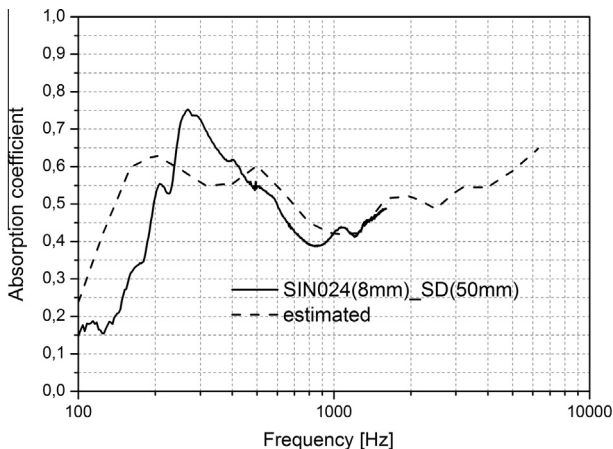


Fig. 20. Estimated and measured absorption behaviour of the layered structure SIN024(8 mm)_SD(50 mm).

thick MEL foam layer. The agreement between the measured and predicted values is good. However, when the 4 mm sintered SIN024 sample layer is backed with a 50 mm SD foam layer, the disagreement between the measured and predicted values (in Fig. 19) is bigger but still satisfactory. Over 10% disagreement is detected at frequencies below 260 Hz and an average of 23% for frequencies between 514 and 986 Hz. When the two layers of sintered sample SIN024 are backed with 50 mm thick SD foam (in Fig. 20), the disagreement between the measured and estimated values is quite poor, on average 45%, at low frequencies, 100–396 Hz. For the frequency range 596–884 Hz, the average disagreement is 14% while for other measured frequencies the agreement is good, with the disagreement under 10%. Below 200 Hz, the impedance tube measurement accuracy again affects the agreement of the estimations. In addition, for SD foam containing layered structures, the estimation accuracy is poorer, a result of the structure differences described in Fig. 15.

4. Conclusions

Novel thin UHMWPE-based micro-porous absorption material is manufactured with the hot-air sintering method to improve absorption at low frequencies. Impedance tube measurement results show that the sintered absorption material layer enhances absorption in the low frequency region. For 4 mm thick material

backed by a 50 mm air gap, the absorption coefficient is above 0.5 starting from 300 Hz and reaching a maximum 0.9 at 600 Hz. Compared with commercial melamine and polyester foam with 50 mm thicknesses, the absorption is clearly better in frequencies below 1000 Hz. As part of the multilayer, the sintered layer enhances absorption at low frequencies. An absorption coefficient above 0.5 is reached at frequencies above 200 Hz with a structure consisting of a 4 mm thick sintered sample layer backed with a 50 mm thick melamine layer.

The NOVA software, based on a mathematical model by Biot's theory, has proved to be a beneficial tool to estimate the behaviour of examined porous materials and structures based on sintered samples, and commercial melamine and polyester foams. For the examined commercial foams, Biot's model gives good agreement between the measured and predicted values if the microstructure of the foam is simple enough. Disagreements of up to 30% are detected with 10 mm thick polyester foam resulting from the complicated microstructure affecting the foam volume subjected to air flow. For sintered samples, the agreement between measured and estimated values is also satisfactory, with the disagreement being below 10% for most of the studied frequency range. Disagreements (maximum 30%) are detected at low frequencies below 300 Hz, especially when the thickness increases. Estimations are sensitive to some modelling parameters, and the measurement accuracy also reduces the estimation accuracy.

Although this preliminary study proves the sintered UHMWPE-based sample layer's capability in absorption applications, more research work is needed to use the sintered sample layer in multi-layer structures. Optimization of the structure could be one solution to cover the broader frequency range. On the modelling side, more research work is needed to determine the effect of different parameters to cover the disagreements between measured and predicted values. Finally, the results can lead to a novel kind of layered sound absorption structures and modelling tools with high performance.

Acknowledgements

This research work was carried out under the NOVI Project. We gratefully acknowledge Tekes—the Finnish Funding Agency for Technology and VTT Technical Research Centre of Finland for their financial support.

References

- [1] Bécot FX, Jaouen L, Gourdon E. Applications of the dual porosity theory to irregularly shaped porous materials. *ACTA Acoust United Acoust* 2008;94: 715–24.
- [2] Perrot C, Chevillotte F, Panneton R. Bottom-up approach for microstructure optimization of sound absorbing materials. *J Acoust Soc Am* 2008;124:940–8.
- [3] Sgard FC, Atalla N, Amedin CK. Vibro-acoustic behavior of a cavity backed by a plate coated with a meso-heterogeneous porous material. *ACTA Acoust United Acoust* 2007;93:106–14.
- [4] Lind E. Predicting and optimising acoustical and vibrational performance of open porous foams. Licentiate Thesis Stockholm, Kungliga Tekniska Högskolan. Department of Aeronautical and Vehicle Engineering, The Marcus Wallenberg Laboratory for Sound and Vibration Research; 2008.
- [5] Arenas JP, Crocker MJ. Recent trends in porous sound-absorbing materials. *Sound Vib* 2010;12–8.
- [6] Forest L, Gibiat V, Hooley A. Impedance matching and acoustic absorption in granular layers of silica aerogels. *J Non-Cryst Solids* 2001;285:230–5.
- [7] Zhou H, Li B, Huang G. Sound absorption behaviour of multiporous hollow micro-spheres. *Mater Lett* 2006;60:3451–6.
- [8] Zhou H, Li B, Huang G. Sound absorption characteristics of polymer microparticles. *J Appl Polym Sci* 2006;101:2675–9.
- [9] Li B, Zhou H, Huang G. A novel impedance matching material derived from polymer micro-particles. *J Mater Sci* 2007;42:199–206.
- [10] Zhou H, Li B, Huang G, He J. A novel composite sound absorber with recycled rubber particles. *J Sound Vib* 2007;304:400–6.
- [11] Swift MJ, Bris P, Horoshenkov KV. Acoustic absorption in re-cycled rubber granulate. *Appl Acoust* 1999;57:203–12.

- [12] Horoshenkov KV, Swift MJ. The effects of consolidation on the acoustic properties of loose rubber granulates. *Appl Acoust* 2001;62:665–90.
- [13] Alderson KL, Evans KE. The fabrication of microporous polyethylene having a negative Poisson's ratio. *Polymer* 1992;33(20):4435–8.
- [14] Alderson KL, Kettle AP, Neale PJ, Pickles AP, Evans KE. The effect of the processing parameters on the fabrication of auxetic polyethylene. *J Mater Sci* 1995;30(16):4069–75.
- [15] Webber RS, Alderson KL, Evans KE. Novel variations in the microstructure of the auxetic microporous ultra-high molecular weight polyethylene. Part 1: Processing and microstructure. *Polym Eng Sci* 2000;40(8).
- [16] Biot M. Theory of propagation of elastic waves in fluid-saturated porous solid. I. Low frequency range. *J Acoust Soc Am* 1956;28(2):168–78.
- [17] Biot M. Theory of propagation of elastic waves in fluid-saturated porous solid. II. Higher frequency range. *J Acoust Soc Am* 1956;28(2):179–91.
- [18] Maa D-Y. Direct and accurate impedance measurement of microperforated panel. IN83; 1983. p. 363–6.
- [19] Maa D-Y. Microperforated_panel wideband absorbers. *NCEJ* 1987;29(3): 77–84.
- [20] Delany M-E, Bazley EN. Acoustical properties of fibrous absorbent materials. *Appl Acoust* 1970;3:105–16.
- [21] Sagartzazu X, Hervella-Nieto L, Pagalday JM. Review in sound absorbing materials. *Arch Comput Methods Eng* 2008;15(3):311–42.